OXFORD

Human Molecular Genetics, 2023, Vol. 32, 9, 1575–1588
https://doi.org/10.1093/hmg/ddac308
Advance access publication date 13 January 2023
Original Article

Methylenetetrahydrofolate reductase deficiency and high-dose FA supplementation disrupt embryonic development of energy balance and metabolic homeostasis in zebrafish

Rebecca Simonian[1,†], Emanuela Pannia[2,†], Rola Hammoud[3], Ramil R. Noche[4], Xiucheng Cui[2], Eva Kranenburg[1], Ruslan Kubant[1], Paula Ashcraft[5], Brandi Wasek[5], Teodoro Bottiglieri[5], James J. Dowling[2] and G. Harvey Anderson[1,6,*]

[1]Department of Nutritional Sciences, Faculty of Medicine, University of Toronto, Toronto, ON M5S 1A8, Canada
[2]Department of Genetics and Genome Biology, Hospital for Sick Children, Toronto, ON M5G 0A4, Canada
[3]Department of Laboratory Medicine and Pathobiology, Lunenfeld-Tanenbaum Research Institute, Mount Sinai Hospital, Toronto ON, M5G 1X5, Canada
[4]Department of Comparative Medicine, Yale Zebrafish Research Core, Yale School of Medicine, New Haven, CT 06511, USA
[5]Baylor Scott & White Research Institute, Institute of Metabolic Disease, Dallas, TX 75204, USA and
[6]Department of Physiology, Faculty of Medicine, University of Toronto, Toronto, ON M5S 1A8, Canada

*To whom correspondence should be addressed, Tel: 416 97818321; Fax: 416 9785882; Email: harvey.anderson@utoronto.ca

†Co-first author.

Abstract

Folic acid (synthetic folate, FA) is consumed in excess in North America and may interact with common pathogenic variants in methylenetetrahydrofolate reductase (MTHFR); the most prevalent inborn error of folate metabolism with wide-ranging obesity-related comorbidities. While preclinical murine models have been valuable to inform on diet–gene interactions, a recent Folate Expert panel has encouraged validation of new animal models. In this study, we characterized a novel zebrafish model of *mthfr* deficiency and evaluated the effects of genetic loss of *mthfr* function and FA supplementation during embryonic development on energy homeostasis and metabolism. *mthfr*-deficient zebrafish were generated using CRISPR mutagenesis and supplemented with no FA (control, 0FA) or 100 μm FA (100FA) throughout embryonic development (0–5 days postfertilization). We show that the genetic loss of *mthfr* function in zebrafish recapitulates key biochemical hallmarks reported in MTHFR deficiency in humans and leads to greater lipid accumulation and aberrant cholesterol metabolism as reported in the M*thfr* murine model. In *mthfr*-deficient zebrafish, energy homeostasis was also impaired as indicated by altered food intake, reduced metabolic rate and lower expression of central energy-regulatory genes. Microglia abundance, involved in healthy neuronal development, was also reduced. FA supplementation to control zebrafish mimicked many of the adverse effects of *mthfr* deficiency, some of which were also exacerbated in *mthfr*-deficient zebrafish. Together, these findings support the translatability of the *mthfr*-deficient zebrafish as a preclinical model in folate research.

Introduction

In utero nutritional and genetic disturbances in folate metabolism predispose to the development of disease risk in later life (1,2). The gene methylenetetrahydrofolate reductase (*MTHFR*) encodes the rate-limiting enzyme in the 1-carbon cycle, producing the only endogenous source of the bioactive folate form 5-methyltetrahydrofolate (5-MTHF) (1). 5-MTHF is integral for homocysteine (Hcy) catabolism, transmethylation reactions and neurotransmission, and is the only folate form that can cross the blood–brain barrier (1,3,4). Rare pathogenic mutations in *MTHFR* underlie severe MTHFR deficiency (*OMIM 607093; c1p36.22*), the most common inborn error of folate metabolism (5,6). To date, a total of 34 mutations have been described in patients with severe MTHFR deficiency, the majority of which are missense mutations in the catalytic N-terminal domain (7). By comparison, up to 50% of the general population contain *MTHFR* variants encoding a thermolabile enzyme with reduced activity (e.g. g.677C > T), underlying a milder form of the disorder (8). Notably, disease consequences associated with both mild and severe MTHFR deficiency are wide-ranging, varying in severity and onset, and include neural tube defects, early and later-life neurobehavioral impairments and/or various cardio-metabolic and immune dysfunctions, including obesity (9–12). This clinical heterogeneity poses a challenge for timely diagnosis and treatment via nutritional therapeutic strategies (e.g. methyl donor supplement) (13–16) and emphasizes a need to identify modifiable risk factors.

To ascertain key elements that limit folate status and contribute to health and disease risk, understanding the interaction between folate intake and *MTHFR* variants is critical. In North America, widespread food fortification and use of prenatal supplements with folic acid (FA, synthetic folate) have been public health strategies for neural tube defect prevention (17), but have also resulted in gestational intakes that may exceed the tolerable upper level (18–20). Consequently, unmetabolized FA (UMFA) has been widely detected in plasma, breast milk and umbilical cord blood (20–24) and may interfere with 1-carbon metabolic processes.

Received: October 7, 2022. **Revised:** December 3, 2022. **Accepted:** December 22, 2022
© The Author(s) 2023. Published by Oxford University Press. All rights reserved. For Permissions, please email: journals.permissions@oup.com

Addressing current gaps in folate research using the rodent model poses challenges and has resulted in the need to validate new animal models for 1-carbon metabolic studies (25). The metabolism of folate is much faster in rodents compared with humans (26) and their use for high-throughput analyses during embryogenesis is limited and costly. Moreover, determining the effects of folate versus UMFA during gestation is not possible because of the confounding effects of the maternal-fetal nutrient supply. By comparison, the zebrafish (*Danio rerio*) offers a unique compromise between *in vivo* complexity and *in vitro* simplicity as it develops rapidly and externally, is optically clear and highly permeable and is readily genetically manipulable (27–29). Most importantly, the folate pathway in zebrafish has been reported to be structurally and kinetically similar to humans, and therefore can be an informative preclinical model for 1-carbon metabolic investigations (30–32).

In this study, our primary objective was to characterize and evaluate the effects of genetic loss of function of *mthfr* and external FA supplementation during embryonic development on energy homeostasis and metabolism in the developing zebrafish. We evaluated energy balance (food intake and metabolic rate), central regulatory gene expression, myeloid cell abundance, lipid accumulation (neutral lipids and cholesterol) and cellular metabolism (1-carbon metabolites). We identify changes consistent with human MTHFR deficiency, thus supporting the suitability of the zebrafish model and system for future folate metabolism and gene–environment studies.

Results

mthfr knockout (KO) in zebrafish does not result in overt morphological differences during embryonic development

In this study, we characterized 4 guide RNA (4gRNA) *mthfr* crispants and zebrafish containing a germline homozygous mutation (*mthfr*−/− mutant zebrafish) via disruption of the 5′ untranslated region (UTR) and transcriptional start site (TSS) of the *mthfr* gene (Fig. 1). The germline mutagenesis approach resulted in a 2058 bp deletion, which included the TSS (Fig. 2A). qRT-PCR confirmed *mthfr* mRNA to be downregulated in whole-4gRNA *mthfr* crispants and *mthfr*−/− zebrafish at 5 days postfertilization (dpf) by ∼60% and ∼80%, respectively, compared with their corresponding controls (Fig. 2B, $P < 0.001$). Both 4gRNA *mthfr* crispants and *mthfr* −/− mutants were viable (Fig. 2C) and did not exhibit gross morphological defects up to 5 dpf (Fig. 2D and E), with no differences noted in body length, body width, jaw length or eye diameter (Supplementary Material, Fig. S1), as well as no observable craniofacial skeleton defects as assayed by Alcian blue stain (Supplementary Material, Fig. S2).

mthfr disruption alters energy regulatory systems during embryonic development

We next measured food intake in first-time exogenously fed zebrafish larvae at both 5 and 8 dpf (via fluorescently labeled paramecia), as well as metabolic rate (via a $NADH_2$ fluorometric assay) in larvae that received no exogenous feeds. At 5 dpf, *mthfr* −/− mutants had lower food intake (∼30%, $P < 0.001$, Fig. 3A–C) and metabolic rate (∼38%, $P < 0.001$, Fig. 3D) compared with wild-type (WT) controls. By comparison, food intake of *mthfr* −/− zebrafish was normalized to that of control by 8 dpf (Fig. 3E–G), whereas metabolic rate remained lower (∼48%, $P < 0.001$, Fig. 3H) highlighting a persistent impact of loss of *mthfr* function on metabolic regulation.

mthfr deficiency reduced central regulatory gene expression

To offer insight into the central regulatory pathways that may be affected by *mthfr* gene disruption, select gene targets previously reported to be sensitive to fluctuations in folate status (33–35) were assayed in heads of *mthfr* −/− versus WT larvae at 5 dpf (Fig. 4). Overall, *mthfr* disruption induced the downregulation of target gene expression. Specifically, lower expression of several genes involved in neurotransmission and neuronal energy regulation was observed in *mthfr* −/− zebrafish including lower *tyrosine hydroxylase* (*th*) (1.3-fold, $P = 0.05$), *dopamine signaling receptor 2a* (*drd2a*) (2-fold, $P < 0.05$), *catechol-o-methyltransferase* (*comta*) (1.5-fold, $P < 0.01$), *gamma-aminobutyric acid type A receptor-4alpha* (*gabra4*) (1.5-fold, $P < 0.05$), *glutamate receptor, ionotropic, N-methyl D-aspartate 1a* (*grin1a*) (1.6-fold, $P < 0.05$) and *brain-derived neurotrophic factor* (*bdnf*) (1.6-fold, $P < 0.01$). mRNA expression of *neuropeptide Y* (*npy*), cocaine- and amphetamine-regulated transcript 4 (*cart4*) and gamma-aminobutyric acid type A receptor-3alpha (*gabra3*) was not affected.

mthfr deficiency in zebrafish affects tissue-specific myeloid cell abundance during embryonic development

Pathogenic variants in *MTHFR* may induce immune cell dysregulation underlying several of the disease consequences (36). We therefore investigated myeloid regulatory cells during embryonic development by generating 4gRNA *mthfr* crispants in the double transgenic line *Tg(mpx:GFP); Tg(mpeg1:mCherry)*. Neutrophil number (as determined by quantifying *mpx:GFP* positive cells) in the dorsal head of both 4gRNA *mthfr* crispants and control larvae was low and did not localize to the central brain region (Supplementary Material, Fig. S3). This is consistent with the limited neutrophil CNS-infiltration seen with an intact blood–brain barrier (37). However, we observed a reduction in the number of macrophages (*mpeg1:mCherry* positive cells) in the dorsal head of 4gRNA *mthfr* crispants compared with cas9 controls (∼25%, $P < 0.01$, Supplementary Material, Fig. S3), suggesting fewer microglia in *mthfr* crispant zebrafish. Notably, myeloid cells in the periphery were not affected at this time as a similar number and distribution pattern of labeled macrophages and neutrophils were observed in crispants and controls both under homeostatic conditions and following a tail-wounding assay (Supplementary Material, Figs S4 and S5). To confirm whether reduced macrophages were reflective of fewer microglia, we performed vital staining with neutral red (NR), a dye that marks microglia, at 4 dpf. Indeed, 4gRNA *mthfr* crispants had ∼20% less NR+ cells in the optic tectum compared with cas9 controls ($P < 0.01$, Fig 5A, B and E). We next corroborated these results in *mthfr* −/− mutant zebrafish and confirmed a similar ∼20% reduction at 4 dpf ($P < 0.001$, Fig. 5C–E) that was maintained to 6 dpf (data not shown). To ascertain whether reduced microglia in *mthfr* −/− zebrafish were because of defects in embryonic macrophage migration, we performed NR staining at 3 dpf (a time point when microglia rapidly populate the midbrain) but found no differences in number or distribution pattern of NR+ cells (data not shown). Microglia in the midbrain are responsible for clearance of dead/apoptotic cells, a process called efferocytosis. Thus, we next investigated whether reduced microglia in *mthfr* −/− mutant zebrafish was a consequence of increased efferocytic demand because of an increase in apoptotic cells. By performing Acridine Orange (AO) staining at 3 dpf, we found that *mthfr*−/− zebrafish had ∼52% more AO+ cells compared with WT ($P < 0.0001$, Fig. 5F–H).

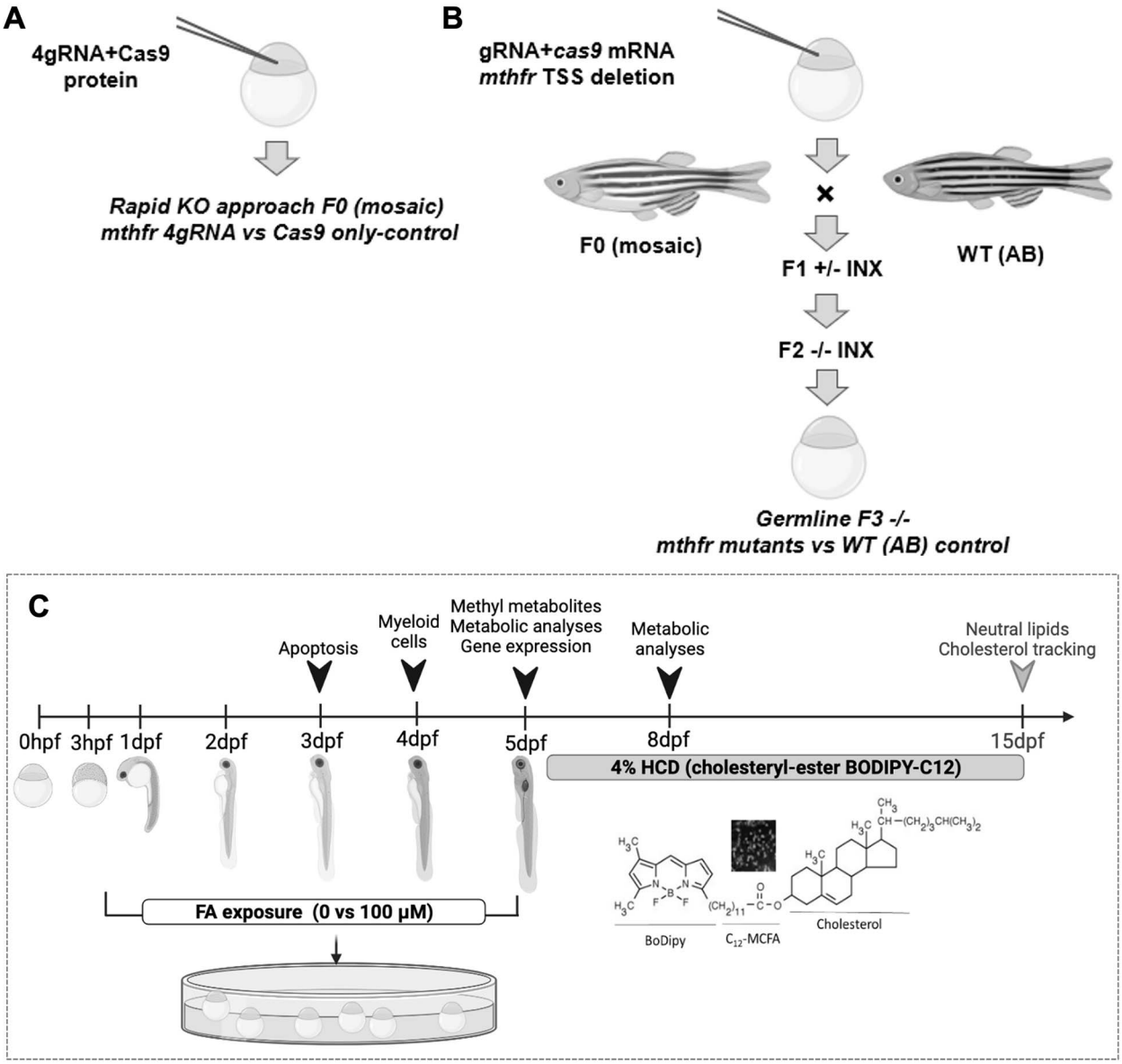

Figure 1. *mthfr* zebrafish model creation and study design. Schematic of the steps to generate (**A**) 4gRNA *mthfr* crispant zebrafish and (**B**) germline *mthfr* −/− mutant zebrafish (HSC194). (**C**) Simplified study design. Metabolic analyses included measures of food intake, metabolic rate and lipid accumulation. Analysis indicated by the gray arrowhead was performed following a 10-day HCD challenge. Abbreviations: F0, mutagenized generation; F1 +/−, first-generation zebrafish heterozygous for *mthfr*; F2 −/−, second-generation zebrafish nullizygous for *mthfr*; hpf, hours postfertilization; MCFA, medium chain fatty acid; WT, wild-type zebrafish from AB background.

Loss of *mthfr* in zebrafish recapitulates a biochemical profile of severe MTHFR deficiency

The folate (Fig. 6A–D) and methyl metabolite (Fig. 6E–L) contents of both 4gRNA *mthfr* crispants and *mthfr* −/− mutants were evaluated to determine whether they mirror the profile reported in severe MTHFR deficiency in humans (38), in support of the observed phenotypic analysis. Accordingly, 4gRNA *mthfr* crispants had ∼80% and *mthfr* −/− mutants had ∼90% lower 5-MTHF concentrations relative to their respective controls ($P < 0.001$, Fig. 6A). The concentration of 5,10-methylenetetrahydrofolate, which interconverts to 5-MTHF, was also lower in both 4gRNA *mthfr* crispants ($P < 0.05$) and *mthfr* −/− zebrafish ($P < 0.01$) compared with controls. The concentrations of synthetic FA, dihydrofolate and 5,10-methenyltetrahydrofolate were below the lower detection limit of quantification for all larvae pools at this time point. Both 4gRNA *mthfr* crispants and *mthfr* −/− zebrafish also had lower concentrations of methionine (MET, $P < 0.05$), and the alternative methyl donor betaine ($P < 0.05$), along with >2-fold higher concentrations of the methyltransferase inhibitor s-adenosylhomocysteine (SAH, $P < 0.01$) and higher cystathionine ($P < 0.01$). The SAM:SAH ratio was also lower in both 4gRNA *mthfr* crispants and *mthfr* −/− zebrafish, likely indicative of reduced methylation potential. Notably, *mthfr* −/− zebrafish also had significantly lower concentrations of tetrahydrofolate (THF) and 5–10-THF, and significantly higher choline and total Hcy concentrations ($P < 0.05$) compared with controls, suggesting a more robust response to *mthfr* disruption on methyl metabolites in the germline model.

Loss of *mthfr* in zebrafish induces lipid dysregulation up to 15 dpf

Next, we explored whether *mthfr* disruption in zebrafish results in the accumulation of lipids, and specifically cholesterol, as has been reported in the *Mthfr* murine model (39–41). We

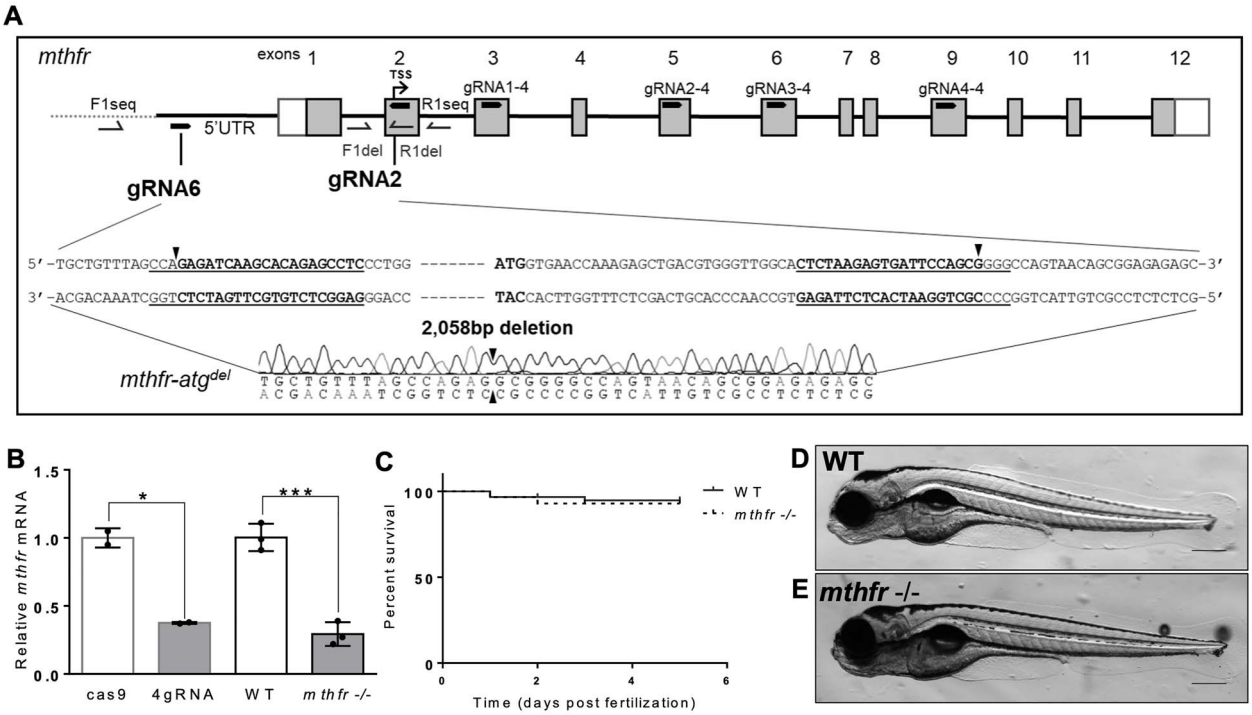

Figure 2. Generation of *mthfr*-deficient zebrafish by CRISPR mutagenesis. (**A**) Schematic representation of the zebrafish genome with guide RNA sequences identified in the *mthfr* gene. The 4gRNA target sequences (gRNA1/2/3/4-4) reside in exons 3, 5, 6 and 9. The two-gRNA approach (gRNA2 and gRNA6) targets sequences in the 5′ UTR and in exon 2, respectively, and results in a 2058 bp deletion (mthfr-atg^{del}) that includes the TSS. Black arrowheads show where gRNA cutting occurred. Boxes indicate exons, with white boxes representing UTR and gray boxes representing protein coding regions. Primer locations used for sequencing are shown. (**B**) Relative *mthfr* mRNA expression in 4gRNA *mthfr* crispants (4gRNA) and *mthfr* −/− mutant zebrafish (*mthfr* −/−, HSC194) compared with their respective controls at 5 dpf. Values are mean ± SEM, $n = 2$–3 biological replicates of $n = 20$ pooled zebrafish/group. Each pool was composed of $n = 20$ larvae. Analyzed by Student's *t*-test. Significant at $^{*}P < 0.05$ and $^{***}P < 0.001$. (**C**) Kaplan–Meier curve showing percent survival of WT and *mthfr* −/− mutant zebrafish larvae throughout embryonic development from 0 to 5 dpf. $n = 60$ larvae/group/petri dish at the start of analysis. (**D**, **E**) Representative image of (D) WT and (E) *mthfr* −/− mutant zebrafish at 5 dpf showing no obvious morphological differences. 10× magnification, scale bar = 200 μm.

first utilized our 4gRNA *mthfr* crispants to perform a long-term *in vivo* CE-BoDipy-C12® fluorescent feeding assay up to 15 dpf. 4gRNA *mthfr* crispants compared with cas9 control zebrafish had greater hepatic accumulation of the fluorescent CE analog ($P < 0.001$, Fig. 7A–G), which has been suggested to reflect aberrant cholesterol metabolism and/or transport (42). A greater percentage (~50%) of 4gRNA *mthfr* crispants also had fluorescent lipid punctae throughout their vasculature ($P < 0.05$, Fig. 7H, Supplementary Material, Video S1) confirming an increased predisposition to vascular lipid accumulation induced by *mthfr* disruptions. Notably, 4gRNA *mthfr* crispants also had greater neutral lipid accumulation, as assessed by Oil-ed-O (ORO) staining, in the viscera region that included the heart and liver area ($P < 0.05$) and in their whole body ($P < 0.05$), accounting for the more intensely stained dorsal artery, intersegmental veins and caudal vein compared with cas9 control zebrafish (Fig. 7I–M). Body length at 15 dpf (data not shown) was not different between zebrafish groups, limiting confounding effects on lipid parameters reported. We next investigated whether *mthfr* disruption resulted in the accumulation of lipids during early development by performing ORO staining in *mthfr* −/− mutants. At 5 dpf, *mthfr* −/− zebrafish had ~75% greater lipid deposition in their vasculature, head and viscera region that included the yolk-sac and heart ($P < 0.0001$, Fig. 7N–P), findings which were persistent up to 8 dpf (Fig. 7Q).

FA supplementation does not rescue and may exacerbate effects of *mthfr* disruption in zebrafish independent of changes in 1-carbon metabolites at 5 dpf

To determine the effect of excess supplemental FA exposure on the developing zebrafish larvae, and to examine the interplay between *mthfr* deficiency and FA supplementation, zebrafish larvae were exposed to either 0 or 100 μm FA up to 5 dpf. FA exposure increased whole-body lipid accumulation, as assessed by ORO staining, in WT and *mthfr* −/− zebrafish as indicated by a significant FA Dose ($P < 0.001$) and Genotype ($P < 0.01$) effect but not an interaction effect (Fig. 8A). Metabolic rate (Fig. 8B) and microglia number (Fig. 8C) were reduced in WT treated with FA to an extent similar to that seen with *mthfr* −/− mutants. By comparisons, food intake (Fig. 8D) of first-time fed zebrafish at 5 dpf was affected by FA Dose ($P < 0.0001$) that was dependent on the Genotype as shown by a significant Genotype × Dose interaction effect ($P < 0.0001$). Specifically, while FA exposure did not affect the amount of food consumed by WT zebrafish at 5 dpf, *mthfr* −/− mutants exposed to FA consumed >50% more food than all other.

As expected, FA was only detected in WT and *mthfr* −/− zebrafish exposed to 100 μm of FA at 5 dpf (Table 1). However, concentrations of methionine, SAM, SAH, SAM:SAH ratio, betaine and choline were unaffected by FA dose as indicated by a

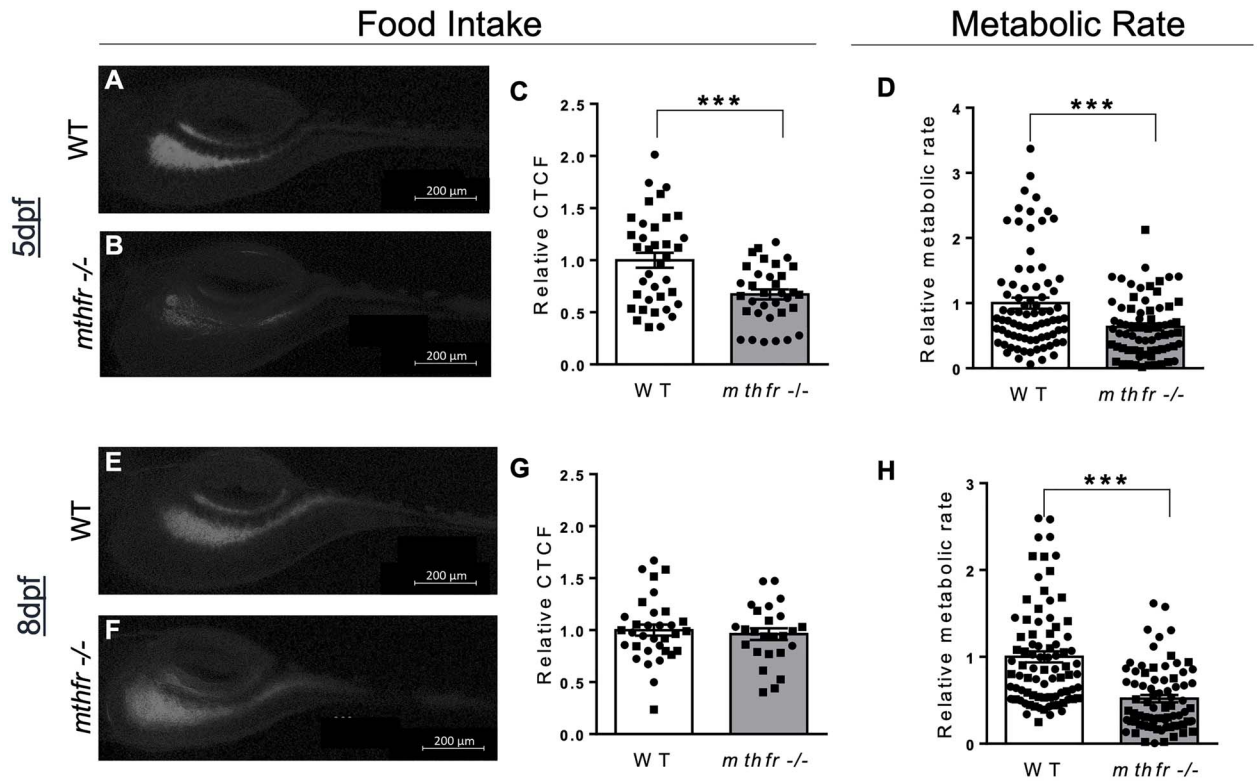

Figure 3. Food intake and metabolic rate are affected by *mthfr* deficiency in larvae. (**A**, **B**) Representative images of zebrafish intestinal content following feeding with fluorescent paramecia in (A) WT controls and (B) *mthfr* −/− mutant zebrafish (*mthfr* −/−, HSC194) at 5 dpf. (**C**) Food intake, measured by relative CTCF, at 5 dpf in WT compared with *mthfr* −/− mutants. (**D**) Relative metabolic rate in WT versus *mthfr* −/− at 5 dpf. (**E**, **F**) Representative images following feeding with fluorescent paramecia in (D) WT and (E) *mthfr* −/− at 8 dpf. (F) Relative CTCF at 8 dpf in WT compared with *mthfr* −/− mutants. (**G**) Relative CTCF at 8 dpf in WT compared with *mthfr* −/− mutants. (**H**) Relative metabolic rate in WT versus *mthfr* −/− at 8 dpf. For all food intake measures: 80× magnification, scale bar = 200 μm, $n = 20$/group. All values are mean ± SEM. Analyzed by Student's *t*-test. Significant at $^{*}P < 0.05$, $^{**}P < 0.01$, $^{***}P < 0.0001$.

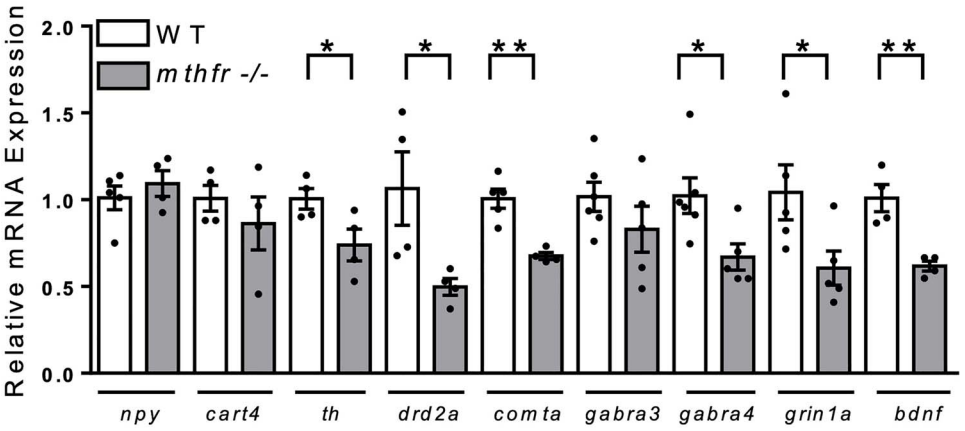

Figure 4. Central regulatory gene expression was altered in *mthfr* −/− at 5 dpf. All values are relative to control. Mean ± SEM, $n = 5$ larval heads/pool, 4–5 pools/group. Analyzed by Student's *t*-test. Significance at $^{*}P < 0.05$, $^{**}P < 0.01$. Abbreviations: *mthfr* −/−, 5-methylenetrahydrofolate reductase homozygous KO germline zebrafish mutants (HSC194); WT, wild-type control zebrafish.

significant Genotype effect ($P < 0.01$) but not by either Dose ($P > 0.05$) or interaction effect. A significant Genotype × Dose interaction was observed on concentrations of cystathionine, with high FA exacerbating *mthfr* deficiency-induced increases.

Discussion

In this study, we generated and characterized a novel model of MTHFR deficiency using the zebrafish and evaluated the effects of *mthfr* deficiency and external FA supplementation during embryonic development on energy homeostasis and metabolism. In *mthfr* zebrafish, energy homeostasis was impaired as indicated by altered food intake, reduced metabolic rate and altered expression of genes involved in regulating food intake in the central nervous system. Microglia abundance was also reduced. Compared with controls, *mthfr* zebrafish had greater hepatic and aortic lipid deposition. Folates, methionine, betaine and SAM:SAH ratio were lower and total Hcy was elevated in *mthfr* zebrafish indicative

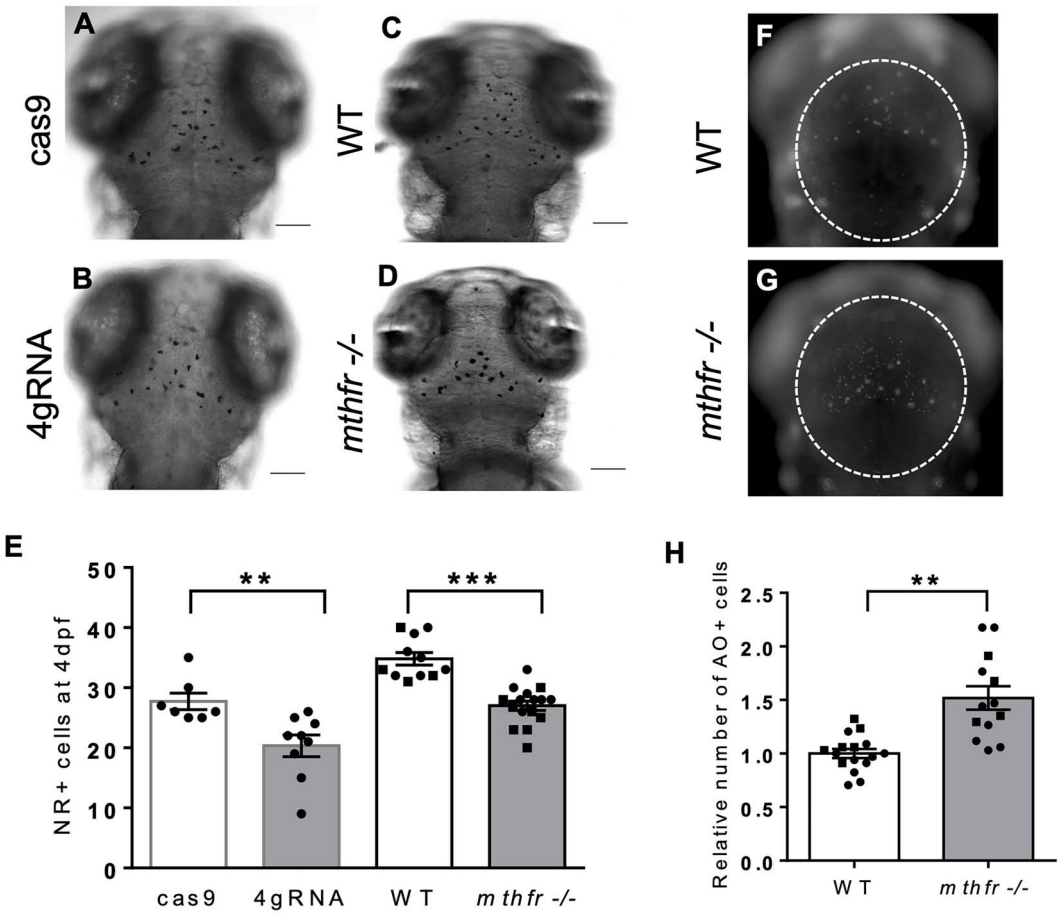

Figure 5. *mthfr* deficiency in zebrafish reduces microglia and increases apoptosis in the optic tectum. (**A**–**D**) Representative bright-field images of NR+ staining at 4 dpf for microglia in (A) cas9, (B) 4gRNA, (C) WT and (D) *mthfr* −/− mutant zebrafish (*mthfr* −/−, HSC194). 80× magnification, scale bar = 100 μm. (**E**) Number of NR+ cells at 4 dpf. $n = 8$–14 larvae/group. Analyzed by one-way ANCOVA with 'batch' as a covariate. Significance at $^{**}P < 0.01$ and $^{***}P < 0.001$. (**F**, **G**) Representative fluorescent images of 3 dpf (F) WT and (G) *mthfr* −/− zebrafish stained with AO. (**H**) Number of AO+ cells at 3 dpf. White dotted line outlines area of quantification. 80× magnification, scale bar = 200 μm. Analyzed by Student's *t*-test. Significant at $^{***}P < 0.001$. All values are mean ± SEM. Circles represent one individual zebrafish from batch 1 and squares represent zebrafish from batch 2.

Table 1. Whole-body methyl metabolite concentrations in larvae exposed to 0 or 100 μm FA up to 5 dpf

	WT						***mthfr* −/−**								
	0 μm FA			**100 μm FA**			**0 μm FA**			**100 μm FA**			**Two-way ANOVA *P*-value**		
Measure	**Mean**	**±**	**SEM**	**Mean**	**±**	**SEM**	**Mean**	**±**	**SEM**	**Mean**	**±**	**SEM**	**D**	**G**	**D × G**
5 dpf															
FA (nmol/g)	<LOD			0.95	±	0.33	<LOD			1.19	±	0.40			
Methionine (nmol/g)	1.00	±	0.15	1.01	±	0.09	0.70	±	0.07	0.77	±	0.07	0.68	**0.03**	0.79
SAM (nmol/g)	1.00	±	0.26	1.54	±	0.12	0.86	±	0.26	1.08	±	0.16	0.09	0.45	0.17
SAH (nmol/g)	1.00	±	0.04	1.32	±	0.15	4.56	±	0.33	4.42	±	0.43	0.78	**<0.0001**	0.47
SAM:SAH (nmol/g)	1.00	±	0.16	1.35	±	0.12	0.26	±	0.07	0.34	±	0.07	0.06	**<0.0001**	0.21
Cystathionine (nmol/g)	1.00[a]	±	0.19	1.09[b]	±	0.05	1.89[a]	±	0.07	2.73[c]	±	0.16	**0.006**	**<0.0001**	**0.02**
Choline (nmol/g)	0.87	±	0.18	0.84	±	0.10	1.22	±	0.09	1.08	±	0.11	0.50	**0.029**	0.68
Betaine (nmol/g)	1.00	±	0.13	1.01	±	0.07	0.70	±	0.04	0.73	±	0.02	0.80	**0.003**	0.85

Values are mean ± SEM, $n = 3$–4 biological replicates of pooled zebrafish/group. Each pool was composed of $n = 50$ larvae for folates and $n = 30$ larvae for methyl metabolites. No differences in pooled weight were observed. Analyzed by two-way ANOVA with FA Dose (0 versus 100 mM) and *mthfr* Genotype (WT versus *mthfr* −/−) as main factors and a Dose × Genotype (D × G) interaction term. Significant at $P < 0.05$. Superscript letters indicate significant differences by Tukey post-hoc analysis. Values in bold indicate significant effects. Abbreviations: *mthfr* −/−, *mthfr* −/− mutant zebrafish (HSC194); WT, wild-type zebrafish.

of reduced methylation potential and consistent with metabolite changes seen in patients with *MTHFR* mutations. In total, these data support the utility of zebrafish as a model for studying MTHFR deficiency and its interplay with early life nutritional environment.

A novel finding of this study is the observed changes in energy homeostasis throughout development in *mthfr* −/−zebrafish up to 8 dpf. We found altered food intake and decreased metabolic rate in *mthfr* −/− zebrafish, which we hypothesized to be driven, in part, by disruption of central energy regulatory pathways.

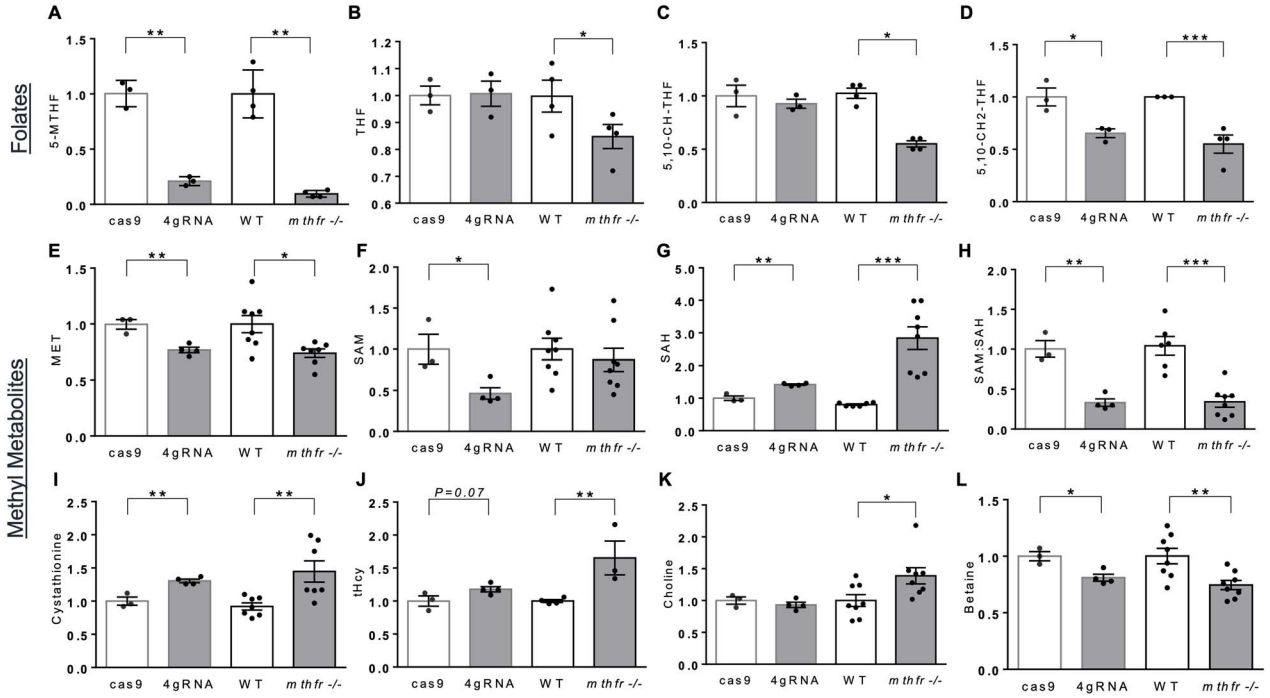

Figure 6. *mthfr* deficiency in zebrafish reduces folates and alters 1-carbon cycle methyl metabolites. Relative concentrations of whole-body (**A**–**D**) folates and (**E**–**L**) related 1-carbon metabolites in zebrafish larvae at 5 dpf. Comparisons were conducted between cas9 versus 4gRNA *mthfr* crispants (4gRNA) or age-matched WT controls versus *mthfr* −/− mutants (*mthfr* −/−, HSC194). Values are mean ± SEM, $n = 3$–4 biological replicates of pooled zebrafish/group. Each pool was composed of $n = 40$ larvae for folates and $n = 20$ larvae for methyl metabolites for cas9 versus 4gRNA *mthfr* crispants and $n = 50$ larvae for folates and $n = 30$ larvae for methyl metabolites for WT versus *mthfr* −/− mutants. No differences in pooled weight were observed. Analyzed by Student's *t*-test stratified by mutagenesis approach. Significant at $^{*}P < 0.05$, $^{**}P < 0.01$, $^{***}P < 0.0001$. Abbreviations: tHcy, total homocysteine; 5,10-CH-THF, 5,10-methenyltetrahydrofolate; 5,10-CH2-THF, 5,10-methylenetetrahydrofolate.

Central regulatory genes that have been previously shown to be targets of maternal folate inadequacies in rodents and/or postulated to be epigenetically modified in patients with MTHFR deficiency (33,34,43) were affected. Overall reductions in central genes involved in dopaminergic (i.e. *drd2a, comta, th*), GABAergic (i.e. *gabra4*) and glutamatergic (i.e. *grin1a*) signaling pathways, as well as those involved in neuronal survival and growth (i.e. *bdnf*) were observed in 5 dpf *mthfr* −/− zebrafish. While the effects of these genes are pleiotropic, they have key roles in regulating the neurotransmission efficiency of central homeostatic and hedonic systems that mediate food intake and energy expenditure (44,45). Downregulation of these signaling genes, as observed in *mthfr* −/− zebrafish, suggests that *mthfr* may act as a regulator of their transcription, and *mthfr* loss may repress related signaling pathways to result in the disease phenotype. Future studies are required to investigate these mechanisms.

mthfr KO in zebrafish also caused a reduction in microglia (likely via increased efferocytic clearance of apoptotic cells) (46) during development, which has important implications in energy balance. Loss of these cells may thus have contributed to widespread energy dysregulation. In zebrafish, microglia are derived from embryonic hematopoietic tissue, colonize the developing brain starting at 2.5 dpf and rapidly populate the midbrain where they are involved in clearance of apoptotic cells, neuronal activity, cellular plasticity and energy metabolism (47). Notably, microglia have been previously shown to be sensitive to changes in folate status as they require 5-MTHF for survival (48) and are directly inhibited by an excess of the neurotoxins SAH and Hcy (49), increases in which were identified in our *mthfr* −/− zebrafish. While the effects of folate fluctuations on microglia abundance during embryonic development in relation to energy metabolism have not been investigated in the murine model, one study reported that the elimination of microglia in the fetal mouse brain resulted in lower *Pomc* neurons and concomitant increases in body weight gain (50). Taken together, our findings support a programming effect of *mthfr* deficiency contributing to disrupted central energy balance regulatory pathways in zebrafish during early life.

Our results also show that *mthfr* deficiency promotes hepatic and aortic accumulation of lipids, and particularly, cholesterol. This is in line with preclinical findings using the *Mthfr* murine model (39,40,51) as well in humans wherein pathogenic variants in *MTHFR* correlate with obesity and cardiometabolic disease risk factors, including dyslipidemia (52,53). During early zebrafish development, the yolk-sac provides a rich lipid reserve to sustain growth up to the exogenous feeding phase (54). As such, lipid accumulation observed in *mthfr* −/− zebrafish during early development likely reflects the onset of atherogenesis in zebrafish (55), and indicates reduced endotrophic lipid consumption (56); findings that may also explain the reduced food intake observed in *mthfr* −/− zebrafish fed exogenously at this time.

The observed energy and metabolic dysregulation in *mthfr* zebrafish may reflect an imbalance in methyl substrates that are key in regulating lipid and energy homeostasis. Our *mthfr* zebrafish reproduced key clinical biochemical hallmarks of severe MTHFR deficiency including increased plasma Hcy and cystathionine and lower plasma methionine (38). This biochemical profile is positively correlated with aberrant lipid profiles and coronary artery disease (57). We also observed several downstream disruptions in the 1-carbon cycle. Increased SAH and reductions in the SAM:SAH ratio and betaine concentrations in *mthfr* zebrafish are in line with reduced methylation potential and increased

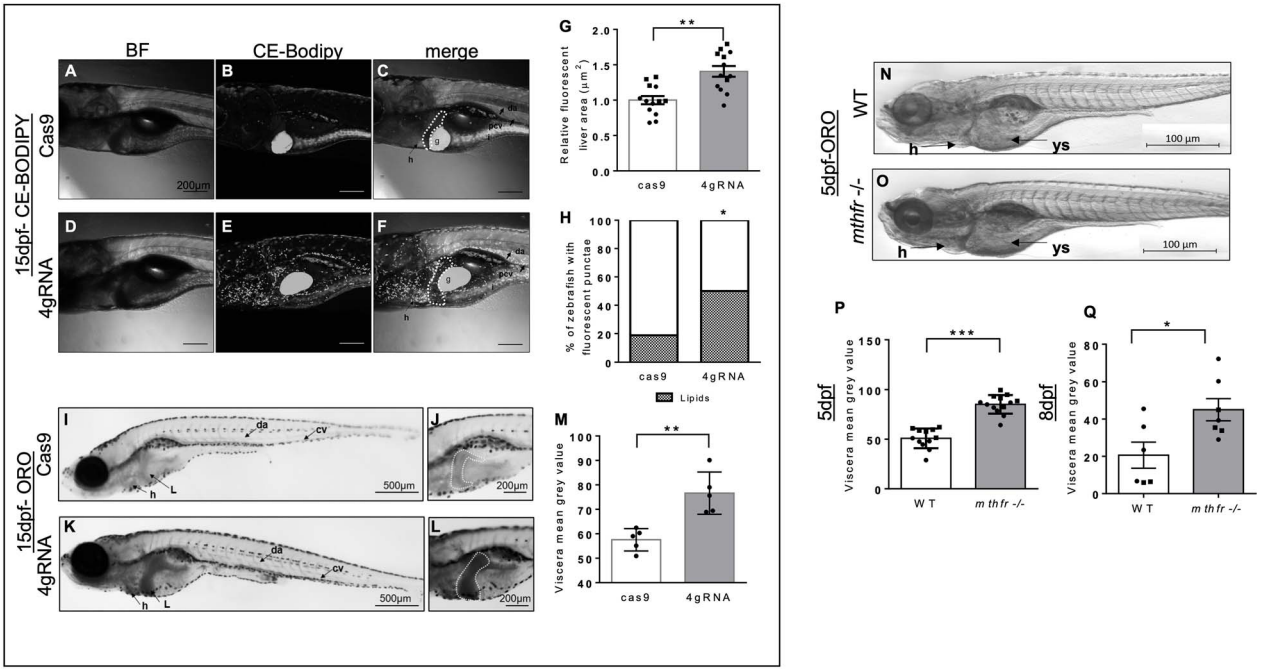

Figure 7. Lipid accumulation is greater in *mthfr* zebrafish compared with controls. (**A**–**F**) Representative bright field (BF) and fluorescent confocal images of (A–C) cas9 control (cas9) and (D–F) 4gRNA *mthfr* crispants (4gRNA) fed a 4% HCD with CE-BoDipy-C12® from 5 to 15 dpf. Fluorescent liver area is outlined by a white dotted line and green fluorescence represents CEs. 10× magnification, scale bar = 200 μm. (**G**) Relative fluorescent liver area and (**H**) percentage of larvae with excess circulating lipids were compared between cas9 and 4gRNA zebrafish. $n = 13$–18 larvae/group. Analyzed by one-way ANCOVA with 'batch' as a covariate. Significance at $^*P < 0.05$. (**I**–**L**) Representative bright-field images of (I, J) cas9 and (K, L) 4gRNA zebrafish stained with ORO at 15 dpf following 10 days of HCD feeding. White dotted line outlines liver area. 20× magnification, scale bar = 500 μm for images I and K and 40× magnification, scale bar = 200 μm for panels J and L. (**M**) Calculated mean gray area of viscera region at 15 dpf. $n = 4$–5 larvae/group. Analyzed by Student's *t*-test. Significance at $^*P < 0.05$, $^{**}P < 0.01$. (**N**, **O**) Representative BF images of WT controls and 5-methylenetrahydrofolate reductase homozygous KO germline zebrafish mutants (*mthfr* −/−, HSC194) at 5 dpf stained with ORO. 20× magnification, scale bar = 500 μm. Calculated mean gray area of viscera region at (**P**) 5 dpf and (**Q**) 8 dpf. $n = 12$–13 larvae/group. Analyzed by one-way ANCOVA with 'batch' as a covariate. Significance at $^*P < 0.05$ and $^{***}P < 0.0001$. Letters and arrows show areas of interest: h, heart; da, dorsal artery; isv, intersegmental area; pcv, posterior cardinal vein; ys, yolk syncytial layer; L, liver; g, gallbladder; i, intestine. All values are mean ± SEM. Circles represent one individual zebrafish from batch 1 and squares represent zebrafish from batch 2.

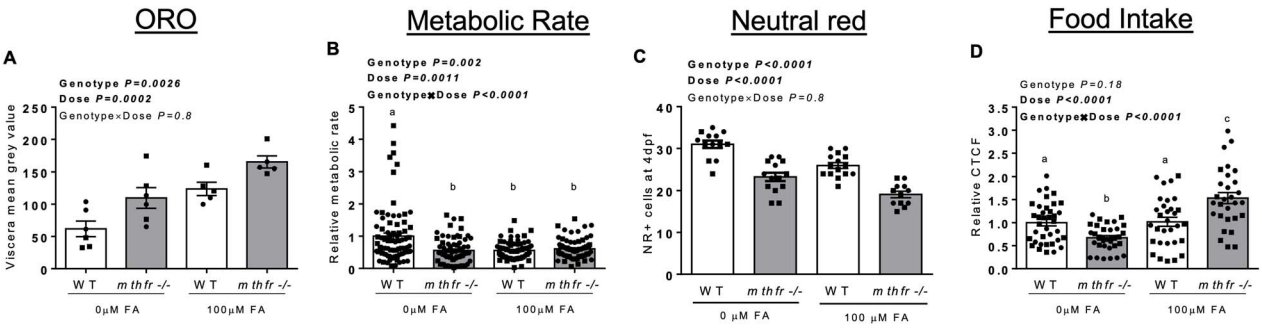

Figure 8. FA dose and *mthfr* genotype interact to affect metabolic outcomes. (**A**) Calculated mean gray area of viscera region at 5 dpf in WT and *mthfr* −/− mutants (*mthfr* −/−, HSC194) exposed to either 0 or 100 mM FA from 0 to 5 dpf and stained with ORO. (**B**) Relative metabolic rate at 5 dpf of WT and *mthfr* −/− exposed to either 0 or 100 mM FA from 0 to 5 dpf. (**C**) Number of NR+ cells at 4 dpf WT and *mthfr* −/− exposed to either 0 or 100 mM FA from 0 to 4 dpf. (**D**) Relative food intake, measured by CTCF, at 5 dpf in WT and *mthfr* −/− exposed to either 0 or 100 mM FA from 0 to 5 dpf. All values are mean ± SEM. Analyzed by two-way ANOVA with FA dose (0 versus 100 mM) and *mthfr* genotype (WT versus *mthfr* −/−) as main factors and a Dose × Genotype interaction term. Significant at $P < 0.05$. Values in bold indicate significant effects. Circles represent one individual zebrafish from batch 1 and squares represent zebrafish from batch 2.

utilization of the betaine-dependent methyl pathway upon functional loss of *mthfr*. This is consistent with findings from human, rodent and other zebrafish studies (58–61) and supports widespread perturbations in methyl metabolism. This altered methyl metabolism may cause dysregulation of the epigenome, and thus aberrant epigenetic modifications, such as via DNA methylation, that may underlie the observed changes in central regulatory gene expression in *mthfr* −/− zebrafish and early and later-life disease consequences of MTHFR deficiency.

An important finding of our study is the phenocopying effects of excess supplemental FA to *mthfr* deficiency in zebrafish. These results hold several important implications. First, while preclinical studies have alluded to the potential adverse effects of excess FA exposure *in utero*, there is limited understanding of the consequences throughout embryogenesis. Our study shows that excess FA may adversely affect cellular energy metabolism and microglia abundance in healthy developing embryos. Second, our results suggest a direct effect of UMFA on the

development of adverse metabolic outcomes during embryogenesis, independent of the maternal contribution to folate status. Third, the adverse effect of UMFA may involve noncanonical folate pathways since FA exposure did not disrupt methyl metabolism. The involvement of UMFA on alternative signaling pathways has been recently hypothesized as an important mechanism of FA-induced pathogenesis, but has not been validated *in vivo* (25).

In this study, we also demonstrate that both *mthfr* crispants and germline *mthfr* −/− mutants show phenotypic and molecular convergence. As crispant analyses are performed directly in the mosaic F0 zebrafish, future experimentation with this model would enable for a high-throughput, rapid and cost-effective screening option to begin to elucidate nutrient–gene interactions and underlying mechanisms mediating mthfr-related pathologies. However, differences between models with respect to key methyl metabolites (e.g. choline, Hcy) highlight the importance of corroborating results in stable biallelic *mthfr* −/− germline zebrafish. Biochemical variability between *mthfr* crispant zebrafish and germline mutants may be explained in part by a maternal effect in the former, and/or the activation of genetic compensation, which was predicted to be reduced in mutants created in this study harboring a TSS deletion (62).

Together, the strength of our study lies in the utility of the *mthfr* zebrafish to address FA knowledge gaps and to advance the understanding of genetic mutation of *mthfr* and the interaction between genotype and the amount and form of supplemental folate during embryogenesis. In addition, the current results have potential application for regulatory decisions and public health advice. Potential adverse outcomes attributed to excess supplemental FA exposures were recently addressed (25) and the findings from our study lend further support. We show adverse effects of UMFA, which may indicate that the use of the natural form of folate, 5-MTHF, should be a priority in maternal supplements, especially during early development of the fetus. In addition, the overriding *mthfr* genotype effect upon exposure to FA, as observed on metabolic rate and methyl metabolites, for example, suggests that treatments with excess FA may have limited therapeutic benefit for *mthfr*-related pathologies, as recently postulated (63). Future dose–response experiments are warranted to elucidate the threshold of possible adverse effects and/or benefits on *mthfr* genotype.

Nevertheless, we also acknowledge that this study has limitations. A main weakness arises from the lack of follow-up on target gene expression within specific brain nuclei, as well as regulatory mechanisms to explain the observed phenotypic changes and pathways related to UMFA actions. Moreover, the lack of standardization of the folate and methyl contents of common zebrafish feeds (e.g. brine shrimp) and limited knowledge of nutrient requirements in zebrafish makes it difficult to perform dietary manipulation studies and infer the contribution of other methyl nutrients to the observed phenotypes. While the FA dose used in this study was informed by past literature (64,65), the standardization of zebrafish nutrient requirements is of high priority to support the use of the zebrafish model for nutrient depletion and exposure studies in the near future.

Both genetic mutation of *mthfr* and FA supplementation affect the development of energy and metabolic homeostasis in zebrafish. These preclinical findings support the translatability of the *mthfr* zebrafish as a preclinical model for folate research and public health applications.

Materials and Methods

Generation of *mthfr*-deficient zebrafish

In collaboration with the Zebrafish Genetics and Disease Models Core Facility at The Hospital for Sick Children (Toronto, Canada), loss of *mthfr* in zebrafish was generated using two CRISPR mutagenesis techniques. To begin assaying for the function of *mthfr in vivo*, a rapid transient KO approach reported to recapitulate germline loss-of-function phenotypes was employed ('Crispants', Fig. 1A) (66). Specifically, 1-cell stage AB WT embryos were injected with 400 pg of Cas9 protein alone (cas9, control, Alt-R® S.p. Cas9 Nuclease V3, IDT, Cat#1081058) or 400 pg of Cas9 protein and a set of 4gRNA at 250 pg each (herein referred to as 4gRNA *mthfr* crispants). 4gRNA targets were adapted from the published genome-scale lookup table for four-guide sets and targeted exons 3, 5, 6 and 9 of the zebrafish *mthfr* gene (Fig. 2A; Supplementary Material, Table S1). For functional validation and characterization of an *mthfr* germline transmitted mutation (*mthfr-atg*^{del}, herein referred to as *mthfr* −/− mutant zebrafish, HSC194, Fig. 1B), 1-cell stage WT embryos were co-injected with 150 pg of Cas9 mRNA and a set of two gRNAs at 100 pg each that were designed to target the 5′ UTR and TSS of the gene located in exon 2 (Fig. 2A). Deletion of the TSS has been previously shown to limit the genetic compensation response induced by the introduction of a premature stop codon by single gRNA injections (62). The gRNA target sites for generation of germline mutants were designed to contain a 20-base pair target sequence using the CRISPR design program Chopchop (http://chopchop.cbu.uib.no/) and are shown in Supplementary Material, Table S1. All gRNAs were synthesized by *in vitro* transcription as previously described (67). Cas9 mRNA was synthesized via *in vitro* transcription from a PCS2 Cas9 vector using the mMessage mMachine SP6 kit (Invitrogen). To evaluate gRNA cutting efficiency, high-resolution melt analysis (HRMA) was performed on a Roche Lightcycler 96 machine using the HRMA master mix kit (Roche) and custom designed primers using PRIMER-BLAST software (Supplementary Material, Table S2). To identify founders (F0s) with germline mutations, sexually mature F0s were outcrossed to WT zebrafish and genomic DNA was isolated from single F1 embryos, PCR amplified and sequence confirmed to determine heterozygous carriers (*mthfr* +/−). As *mthfr* is a maternally inherited transcript, F1 sequence confirmed that *mthfr* +/− mutants were in-crossed to generate F2 *mthfr* homozygous (−/−) mutants, which were confirmed by PCR amplification. PCR sequencing primers (Fig. 2A; Supplementary Material, Fig. S1; Supplementary Material, Table S2) were designed to amplify a 2308 bp product in WT zebrafish, a 250 bp product in heterozygous zebrafish and to result in no amplification in homozygous zebrafish. All *mthfr* disruptions were also validated at the transcript level by qRT-PCR using pooled samples of whole larvae ($n = 20$/pool × 3 pools/group) at 5 dpf (Supplementary Material, Table S3). Levels of 5-MTHF, which requires a functional *mthfr* transcript, were quantified by liquid chromatography tandem mass spectrometry (LC-MS/MS) as described below. Progenies from the F2 or F3 adult *mthfr* −/− in-cross (INX) were used for characterization in this study. Progenies generated from age-matched WT zebrafish maintained under identical conditions were used as controls. All mating pairs were between the age of 6 and 8 months.

Study design

A simplified schematic of the study design is depicted in Figure 1C. 4gRNA *mthfr* crispants and/or *mthfr* −/− mutant

zebrafish and their respective controls (cas9 and WT) were exposed to either no FA (0 μm, control) or a supplemental dose of 100 μm FA in their water during their endogenous feeding phase (up to 5 dpf) and phenotypic and molecular analyses were conducted. For analyses during the exogenous feeding phase (>5 dpf), zebrafish larvae were either fasted or fed a high cholesterol diet (HCD) up to 15 dpf with or without fluorescent cholesteryl (CE)-BODIPY-C12. A power analysis was performed *a priori* to determine the sample size required for food intake ($n = 20$–24/batch), metabolic rate ($n = 40$–45/batch) and remaining analyses ($n = 5$–8/batch). All experiments were replicated at least twice or more unless indicated and methods were conducted as detailed below. Because of the small size of the zebrafish larvae, pooled samples were used for qRT-PCR and biochemical analyses. All analyses were conducted in a blinded manner.

Zebrafish husbandry

All adult zebrafish were maintained at 28.5°C under a 14:10-h light/dark cycle at the Zebrafish Facility at SickKids Peter Giligan Center for Research and Learning (Toronto, CA), and experiments were approved by the SickKids Animal Care Committee (AUP Protocol #56033). Adult zebrafish (>60 days) used for breeding were fed live brine shrimp (*Artemia salina*; containing ~90% moisture, 50% protein, 15% lipids, 15% carbohydrates, 3.5% fiber and 15–20% ash, % dry weight) twice daily (68,69). Of note, the folate content of brine shrimp has previously been reported to be ~0.0007 mg/g. Breeding pairs (2 female: 2 male) were set up with dividers following the last feed of the day. From 0 to 5 dpf, embryos were maintained in a 28.5°C incubator in embryo water (60 μg/ml Instant Ocean® sea salt in system water, pH = 7.7) containing 0.1% methylene blue or when indicated, maintained in 0.003% 1-phenyl 2-thiourea (PTU) in autoclaved system water to inhibit pigmentation. Water was changed daily to ensure sterile conditions. The 0–5 dpf early developmental period of the zebrafish represents the endogenous feeding phase wherein nutrients are obtained from their maternally loaded yolk-sac (54). Notably by 1 dpf, the zebrafish embryo had no detectable levels of synthetic FA as determined by LC-MS/MS (data not shown), limiting confounding effects of the maternal nutrient supply on outcome measures.

FA exposure

Embryos ($n = 20$ embryos/group) were collected 3 h after the onset of mating, staged according to Kimmel *et al.* (27) and exposed to FA (Sigma) at a dose of either 0 μm (0FA, control exposure) or 100 μm (100FA, high) up to 5 dpf. The 3-h time point was chosen as the zebrafish genome is globally re-methylated following fertilization at this time (70). FA solutions were prepared fresh daily in the dark using autoclaved system water. All petri dishes were sealed with parafilm, wrapped in aluminum foil and left in the incubator undisturbed for each consecutive 24-h period. Of note, the 100 μm dose of FA was chosen as it has been shown to impair the activity of the rate limiting enzyme for FA metabolism, dihydrofolate reductase in zebrafish, similar to humans (64). No teratogenicity has been reported in zebrafish exposed to this dose during development (65), which was confirmed by our group following a preliminary dose response experiment.

Intestinal food intake quantification

Intestinal food intake was measured in first-time fed 5 and 8 dpf zebrafish larvae raised in PTU according to the protocol by Wee *et al.* (71) with slight modifications. Paramecia were incubated with a lipophilic tracer (DiD' solid, D-7757, Thermo Fisher Scientific, dissolved in ethanol) for 2 h with mild agitation. Zebrafish were habituated in small petri dishes (35 × 15 mM) for at least 2 h ($n = 20$ larvae/dish) and subsequently exposed to an abundance of labeled paramecia for 3 h in the incubator. Following feeding, larvae were thoroughly washed to remove excess paramecia, transferred to a clean petri dish with PTU water and anesthetized with 0.003% tricaine. Samples were mounted in 3% methylcellulose in autoclaved system water on a single cavity depression slide and imaged using a Zeiss Axio Zoom macroscope. ImageJ was used to calculate corrected total cell fluorescence (CTCF): CTCF = Integrated Density – (Area of selected cell × Mean fluorescence of background readings). Animals that did not feed (as indicated by no fluorescence) were not included in final analyses.

Metabolic rate

Metabolic rate assessment was performed according to a protocol by Williams and Renquist (72) wherein $NADH_2$ production was measured as a proxy for energy expenditure. Briefly, 5 and 8 dpf zebrafish larvae were plated individually into a 96-well plate with 300 μL of assay solution containing alamarBlue™ Cell Viability Reagent (ThermoFisher Scientific Cat #: A50100). Blank wells containing only assay solution served as controls. Baseline fluorescence was measured using a fluorescent plate reader with excitation and emission wavelengths at 530 and 590 nm, respectively. The plate was wrapped in aluminum foil to avoid photobleaching and placed in a 28.5°C incubator overnight. Fluorescence was measured 24 h later. Change in fluorescence was calculated as follows: fluorescence (24 h) – fluorescence (baseline). The average change in fluorescence of the blank wells was subtracted from each well of interest. Lastly, the relative change in fluorescence was calculated as follows: Change in fluorescence (well of interest)/Average change in fluorescence (WT wells).

Central energy regulatory gene expression

To begin to explore the effects of *mthfr* disruption on central energy regulation, we performed qRT-PCR for select energy regulatory transcripts using pooled samples of dissected larval heads with eyes removed ($n = 5$ heads/pool × 5 pools/group). The targets chosen were adapted from our previous study in rats (33,34) and others using the *Mthfr* mouse model (35) whereby they have been shown to be sensitive to folate fluctuations. Targets included: the orexigenic *npy* and anorectic *cart4*; and genes involved in neurotransmission of energy regulating neurons: *th*, *drd2a*, *comta*, *gabra3*, *gabra4*, *grin1a* and *bdnf*. Total RNA was extracted using Trizol reagent and quantified using a NanoDrop™ 2000 spectrophotometer. cDNA synthesis was conducted using the High Capacity cDNA Reverse Transcriptase Kit (Applied Biosystems Inc., catalog #: 4368813). qRT-PCR was performed using SYBR Green (ThermoFisher, catalog #: A25742) on the Roche Lightcycler 96 machine. mRNA levels were normalized to levels of *b-actin* as the housekeeping gene selected based on lowest variation as the control. Primers were designed using PRIMER-BLAST software as listed in Supplementary Material, Table S3. The $2^{-\Delta\Delta}$CT method was used for all analyses (73).

In vivo myeloid cell analyses and tail wounding assay

Immune dysfunction has been suggested to be an underlying pathophysiology for diseases associated with pathogenic variants in MTHFR (36). As such, we explored whether *mthfr* disruption in zebrafish affected myeloid regulatory cells during embryonic development. 4gRNA + Cas9 protein or Cas9-only was co-injected into 1-cell stage zebrafish embryos generated from the INX of a double transgenic line expressing green fluorescent protein (GFP) under the control of a myeloid-specific peroxidase promoter (*mpx*)

to highlight neutrophils [*Tg(mpx:GFP)*^{i114}] (74), and red fluorescent protein (mCherry) under the macrophage expressed gene 1 promoter (*mpeg1*) to visualize macrophages [*Tg(mpeg1:mCherry)*^{gl23}] (75). To test the effects of neutrophil chemotaxis upon tissue injury, a tail fin wounding assays was performed as previously described (76). Z-stacks were captured through the entire dorsal head region or the left–right axis of the zebrafish trunk using a Nikon A1 confocal microscope.

In addition, NR vital staining was performed for visualization of microglia at 3, 4, and 6 dpf using freshly prepared NR solution with PTU autoclaved system water (5 μg/mL, Sigma, catalog #: N-4638) as previously described (46). For each experiment, equal larvae per petri dish containing 25 mL of NR solution were incubated in the dark at 28.5°C for 2 h. Following incubation, larvae were rinsed in PTU autoclaved system water for 20 min, anesthetized with tricaine (0.16 mg/ml) and mounted in 3% methylcellulose on a single cavity depression slide for analysis using a Zeiss Axio Zoom. ImageJ was used to count the number of NR+ cells.

AO staining

As an index of apoptosis, the vital dye AO (Invitrogen™, catalog #: A1301) dye was used (77). Briefly, larvae were raised to 3 dpf in PTU autoclaved system water. At 3 dpf, larvae ($n = 10$/group) were stained with 2.5 μg/mL of AO in PTU system water for 20 min, thoroughly washed and imaged in the GFP channel using the Zeiss Axio Zoom. ImageJ was used to count the number of AO+ cells.

In vivo cholesterol tracking

In vivo analysis of cholesterol metabolism was conducted in 4gRNA *mthfr* crispants using a CE-BODIPY-C12® fluorophore (ThermoFisher, catalog #: D3822) as previously described (78–80). Briefly, embryos ($n = 13$/group) were transferred to a 1.6 L tank at 5 dpf and fed equal quantities (equating to 0.3 g of food/larvae/day) of the AP-100 larvae zebrafish diet (crude protein min 50.0%, crude fat min 12.0%, crude fiber max 2.5%, moisture max 10.0%, ash max 15.0%, phosphorus min 1.3%, Ziegler, 50 μm size) with added 4% w/w cholesterol (HCD) up to 13 dpf. Larvae were then fed the HCD supplemented with 1 μg/g of CE-BODIPY-C12® until 15 dpf. The HCD helped stimulate native enzymes required for cholesterol metabolism to enable the incorporation of the CE-BODIPY-C12® fluorophore. Live 15 dpf zebrafish were then mounted in 1.5% low-melting agarose containing tricaine on a 3 cm glass-bottom petri dish and z-stacks were taken using a Nikon Eclipse Ti confocal microscope using a 10× objective lens. Maximum Z-stack projections of equal size were analyzed on ImageJ to measure total liver area (mm^2) and fluorescent intensities.

Neutral lipid analyses

Total neutral lipid accumulation was investigated via ORO staining starting at 5 dpf, when yolk-derived lipids are being absorbed (54), followed by 8 dpf, when yolk-sac lipid absorption is predicted to be completed (81) and then at 15 dpf (n = 5 larvae/group) following a HCD challenge. Briefly, 5 and 8 dpf larvae raised in PTU were fixed in 4% paraformaldehyde overnight at 4°C and washed 3x for 5 min with 1X-PBS-0.5% Tween (1X-PBST). Larvae were then stained with 300 μL of filtered 0.5% ORO dissolved in 100% isopropanol and 200 μL of distilled water for 15 min. Larvae were washed with 1X-PBST 3x for 5 min, 2x in 60% isopropanol for 5 min and 1x in 1X-PBST for 5 min. For 15pf larvae, bleach was used to remove pigmentation. A bleaching solution was made using equal volumes of 3% H_2O_2 and 2% KOH for a final concentration of 1.5% H_2O_2 and 1% KOH. Upon removal of stain, 1 mL of freshly prepared bleach solution was added to samples in microcentrifuge tubes with lids opened at room temperature for 10 min, followed by 3x washes in 1X-PBST. Samples were transferred into 80% glycerol and mounted onto a single cavity depression slide for analysis using Zeiss Axio Zoom. The mean gray area of a region of interest was quantified on ImageJ.

Folates and methyl metabolites

Concentrations of folate derivatives and methyl metabolites were measured at 5 dpf when yolk-sac nutrient stores have begun depletion. For folates, liquid chromatography coupled with electrospray positive ionization tandem mass spectrometry (LC-ESI-MS/MS) was performed as previously described with minor modifications (82). Briefly, equal pools of zebrafish larvae ($n = 50$ per pool × 4 pools/group) were sonicated in 250 μL of extraction buffer (HEPES buffer pH 8) to which charcoal treated rat plasma was added as a source of pteroylpolyγglutamate hydrolase for the deconjugation of the polyglutamate forms to monoglutamate forms of folates. Following centrifugation, filtering and addition of $^{13}C_5$-methyl-THF internal standard (IS), clear extracts were injected in the UHPLC-MS/MS system consisting of a Waters Acquity UPLC coupled to a Xevo-TQS triple quadrupole mass spectrometer equipped with an electrospray ionization probe (Waters Corporation, Milford, MA, USA). Quantification of folate forms was achieved using the peak area ratio (area of metabolite/area of IS). Concentrations of methionine, s-adenosylmethionine (SAM), SAH, Hcy, cystathionine, choline and betaine in whole-zebrafish larvae were determined by LC-ESI-MS/MS. Pooled zebrafish larvae ($n = 30$/pool × 4 pools/group) were sonicated with 100 μL of methanol, spun for 10 min and 40 μL of the supernatant was dried down under nitrogen for 5 min. Samples were then reconstituted in 40 μL of mobile phase A and diluted 1:5 with IS. Extracts were loaded into the LC-MS/MS system (QTrap 5500, Sciex, Framingham, MA) and metabolites quantitated using Analyst 6.0 (Sciex, Framingham, MA). Data points that were below the lower limit of detection were not included in statistical analysis.

Statistical analysis

All statistical analyses were conducted using SAS version 9.4. A Student's *t*-test was used to determine differences between control and *mthfr* disrupted zebrafish with stratification based on method of mutagenesis. When experiments were conducted in replicates, a one-way ANCOVA using the PROC GLIMMIX procedure was used to control for variance between days of sample collections. To compare the effects of *mthfr* genotype and FA dose, a two-way ANOVA was used with Genotype and Dose as main effects and a Genotype × Dose interaction effect. Significant interaction effects were followed by Tukey's post-hoc test for pairwise comparisons. All significance is reported at $P < 0.05$ and all values are expressed as mean ± SEM. All sample data points were included in each analysis unless stated otherwise.

Supplementary Material

Supplementary Material is available at *HMG* online.

Conflicts of Interest statement: None declared.

Funding

The Canadian Institutes of Health Research, Institute of Nutrition, Metabolism and Diabetes (Grant No.); the Natural Sciences and Engineering Research Council of Canada (Grant No.).

Data Availability

All data supporting the findings of this study are available within the article and its supplementary materials. The data that support the findings of this study are also available upon request from the corresponding author, GHA.

Authors' Contributions

R.S., E.P., R.H., R.K., R.R.N. and G.H.A. contributed to study design; R.S., E.P. and X.C. performed zebrafish experiments; R.S., E.P., R.H. and E.K. analyzed data; P.A., B.W. and T.B. were responsible for LCMS analyses; J.J.D. and G.H.A. provided essential reagents and materials; R.S., E.P., R.H., J.J.D. and G.H.A. contributed to manuscript preparation; R.S., E.P., J.J.D. and G.H.A. had primary responsibility for final content. All authors read and approved the final manuscript.

References

1. Ducker, G. and Rabinowitz, J.D. (2017) One-carbon metabolism in health and disease. *Cell Metab.*, **25**, 27–42.
2. Zheng, Y. and Cantley, L.C. (2019) Toward a better understanding of folate metabolism in health and disease. *J. Exp. Med.*, **216**, 253–266.
3. Stover, P.J., Durga, J. and Field, M.S. (2017) Folate nutrition and blood–brain barrier dysfunction. *Curr. Opin. Biotechnol.*, **44**, 146–152.
4. Scaglione, F. and Panzavolta, G. (2014) Folate, folic acid and 5-methyltetrahydrofolate are not the same thing. *Xenobiotica*, **44**, 480–488.
5. Schwahn, B. and Rozen, R. (2001) Polymorphisms in the methylenetetrahydrofolate reductase gene: clinical consequences. *Am. J. Pharmacogenomics*, **1**, 189–201.
6. Froese, D.S., Huemer, M., Suormala, T., Burda, P., Coelho, D., Guéant, J.L., Landolt, M.A., Kožich, V., Fowler, B. and Baumgartner, M.R. (2016) Mutation update and review of severe methylenetetrahydrofolate reductase deficiency. *Hum. Mutat.*, **37**, 427–438.
7. Leclerc, D., Sibani, S. and Rozen, R. Molecular biology of methylenetetrahydrofolate reductase (MTHFR) and overview of mutations/polymorphisms. In *Madame Curie Bioscience Database*. Landes Bioscience, Austin, TX. 2000–2013. Available from: https://www.ncbi.nlm.nih.gov/books/NBK6561/.
8. Sibani, S., Leclerc, D., Weisberg, I.S., O'Ferrall, E., Watkins, D., Artigas, C., Rosenblatt, D.S. and Rozen, R. (2003) Characterization of mutations in severe methylenetetrahydrofolate reductase deficiency reveals an FAD-responsive mutation. *Hum. Mutat.*, **21**, 509–520.
9. Huemer, M., Mulder-Bleile, R., Burda, P., Froese, D.S., Suormala, T., Zeev, B., Chinnery, P.F., Dionisi-Vici, C., Dobbelaere, D., Gökcay, G. *et al.* (2016) Clinical pattern, mutations and in vitro residual activity in 33 patients with severe 5, 10 methylenetetrahydrofolate reductase (MTHFR) deficiency. *J. Inherit. Metab. Dis.*, **39**, 115–124.
10. Aljassim, N., Alfadhel, M., Nashabat, M. and Eyaid, W. (2020) Clinical presentation of seven patients with methylenetetrahydrofolate reductase deficiency. *Mol. Genet. Metab. Reports.*, **25**, 100644.
11. Gales, A., Masingue, M., Millecamps, S., Giraudier, S., Grosliere, L., Adam, C., Salim, C., Navarro, V. and Nadjar, Y. (2018) Adolescence/adult onset MTHFR deficiency may manifest as isolated and treatable distinct neuro-psychiatric syndromes. *Orphanet J. Rare Dis.*, **13**, 1–8.
12. Marelli, C., Lavigne, C., Stepien, K.M., Janssen, M.C.H., Feillet, F., Kožich, V., Jesina, P., Schule, R., Kessler, C., Redonnet-Vernhet, I. *et al.* (2021) Clinical and molecular characterization of adult patients with late-onset MTHFR deficiency. *J. Inherit. Metab. Dis.*, **44**, 777–786.
13. Knowles, L., Morris, A.A.M. and Walter, J.H. (2016) In Morava, E., Baumgartner, M., Patterson, M., Rahman, S., Zschocke, J. and Peters, V. (eds), *Treatment with Mefolinate (5-Methyltetrahydrofolate), but Not Folic Acid or Folinic Acid, Leads to Measurable 5-Methyltetrahydrofolate in Cerebrospinal Fluid in Methylenetetrahydrofolate Reductase Deficiency*. Springer Berlin Heidelberg, Berlin, Heidelberg, pp. 103–107.
14. Prinz-Langenohl, R., Brämswig, S., Tobolski, O., Smulders, Y., Smith, D., Finglas, P. and Pietrzik, K. (2009) [6S]-5-methyltetrahydrofolate increases plasma folate more effectively than folic acid in women with the homozygous or wild-type 677C→T polymorphism of methylenetetrahydrofolate reductase. *Br. J. Pharmacol.*, **158**, 2014–2021.
15. Servy, E.J., Jacquesson-Fournols, L., Cohen, M. and Menezo, Y.J.R. (2018) MTHFR isoform carriers. 5-MTHF (5-methyl tetrahydrofolate) vs folic acid: a key to pregnancy outcome: a case series. *J. Assist. Reprod. Genet.*, **35**, 1431–1435.
16. Diekman, E.F., De Koning, T.J., Verhoeven-Duif, N.M., Rovers, M.M. and Van Hasselt, P.M. (2014) Survival and psychomotor development with early betaine treatment in patients with severe methylenetetrahydrofolate reductase deficiency. *JAMA Neurol.*, **71**, 188–194.
17. Crider, K.S., Bailey, L.B. and Berry, R.J. (2011) Folic acid food fortification-its history, effect, concerns, and future directions. *Nutrients*, **3**, 370–384.
18. Gómez, M.F., Field, C.J., Olstad, D.L., Loehr, S., Ramage, S., Mccargar, L.J. and the APrON Study Team (2015) Use of micronutrient supplements among pregnant women in Alberta: results from the Alberta pregnancy outcomes and nutrition (APrON) cohort. *Matern. Child Nutr.*, **11**, 497–510.
19. Sullivan, K.M., Ford, E.S., Azrak, M.F. and Mokdad, A.H. (2009) Multivitamin use in pregnant and nonpregnant women: results from the behavioral risk factor surveillance system. *Public Health Rep.*, **124**, 384–390.
20. Plumptre, L., Masih, S.P., Ly, A., Aufreiter, S., Sohn, K.J., Croxford, R., Lausman, A.Y., Beerger, H., O'Connor, D.L. and Kim, Y. (2015) High concentrations of folate and unmetabolized folic acid in a cohort of pregnant Canadian women and umbilical cord blood. *Am. J. Clin. Nutr.*, **102**, 848–857.
21. Pfeiffer, C.M., Sternberg, M.R., Fazili, Z., Yetley, E.A., Lacher, D.A., Bailey, R.L. and Johnson, C.L. (2015) Unmetabolized folic acid is detected in nearly all serum samples from us children, adolescents, and adults. *J. Nutr.*, **145**, 520–531.
22. Stamm, R.A., March, K.M., Karakochuk, C.D., Gray, A.R., Brown, R.C., Green, T.J. and Houghton, L.A. (2018) Lactating Canadian women consuming 1000 μg folic acid daily have high serum folic acid above a threshold concentration of serum total folate. *J. Nutr.*, **148**, 1103–1108.
23. Page, R., Robichaud, A., Arbuckle, T.E., Fraser, W.D. and MacFarlane, A.J. (2017) Total folate and unmetabolized folic acid in the breast milk of a cross-section of Canadian women. *Am. J. Clin. Nutr.*, **105**, 1101–1109.
24. Houghton, L.A., Yang, J. and O'Connor, D.L. (2009) Unmetabolized folic acid and total folate concentrations in breast milk are unaffected by low-dose folate supplements. *Am. J. Clin. Nutr.*, **89**, 216–220.
25. Maruvada, P., Stover, P.J., Mason, J.B., Bailey, R.L., Davis, C.D., Field, M.S., Finnell, R.H., Garza, C., Green, R., Gueant, J. *et al.*

(2020) Knowledge gaps in understanding the metabolic and clinical effects of excess folates/folic acid: a summary, and perspectives, from an NIH workshop. *Am. J. Clin. Nutr.*, **112**, 1390–1403.
26. Bailey, S.W. and Ayling, J.E. (2009) The extremely slow and variable activity of dihydrofolate reductase in human liver and its implications for high folic acid intake. *Proc. Natl. Acad. Sci. U. S. A.*, **106**, 15424–15429.
27. Kimmel, C.B., Ballard, W.W., Kimmel, S.R., Ullmann, B. and Schilling, T.F. (1995) Stages of embryonic development of the zebrafish. *Dev. Dyn.*, **203**, 253–310.
28. Haffter, P., Granato, M., Brand, M., Mullins, M.C., Hammerschmidt, M., Kane, D.A., Odenthal, J., van Eeden, F.J., Jiang, Y.J., Heisenberg, C.P. *et al.* (1996) The identification of genes with unique and essential functions in the development of the zebrafish, *Danio rerio*. *Development*, **123**, 1–36.
29. Driever, W., Schier, A.F., Neuhauss, S.C.F., Malicki, J., Stemple, D.L. and Stainier, D.Y.R. (1996) A genetic screen for mutations affecting embryogenesis in zebrafish. *Development*, **123**, 37–46.
30. Lee, M.S., Bonner, J.R., Bernard, D.J., Sanchez, E.L., Sause, E.T., Prentice, R.R., Burgess, S.M. and Brody, L.C. (2012) Disruption of the folate pathway in zebrafish causes developmental defects. *BMC Dev. Biol.*, **12**, 12.
31. Tu, H.C., Lee, G.H., Hsiao, T.H., Kao, T.T., Wang, T.Y., Tsai, J.N. and Fu, T.F. (2017) One crisis, diverse impacts - tissue-specificity of folate deficiency-induced circulation defects in zebrafish larvae. *PLoS One*, **12**, 1–23.
32. Lee, G.H., Cheng, N.W., Yu, H.H., Tsai, J.N., Liu, T., Wen, Z.H., Chen, B.H. and Fu, T.F. (2019) A novel zebrafish model to emulate lung injury by folate deficiency-induced swim bladder defectiveness and protease/antiprotease expression imbalance. *Sci. Rep.*, **9**, 1–12.
33. Pannia, E., Hammoud, R., Kubant, R., Sa, J.Y., Simonian, R., Wasek, B., Ashcraft, P., Bottiglieri, T., Pausova, Z. and Anderson, G.H. (2021) High intakes of [6S]-5-methyltetrahydrofolic acid compared with folic acid during pregnancy programs central and peripheral mechanisms favouring increased food intake and body weight of mature female offspring. *Nutrients*, **13**, 1477.
34. Pannia, E., Hammoud, R., Simonian, R., Arning, E., Ashcraft, P., Wasek, B., Bottiglieri, T., Pausova, Z., Kubant, R. and Anderson, G.H. (2021) [6S]-5-methyltetrahydrofolic acid and folic acid pregnancy diets differentially program metabolic phenotype and hypothalamic gene expression of Wistar rat dams post-birth. *Nutrients*, **13**, 48.
35. Jadavji, N.M., Wieske, F., Dirnagl, U. and Winter, C. (2015) Methylenetetrahydrofolate reductase deficiency alters levels of glutamate and γ-aminobutyric acid in brain tissue. *Mol. Genet. Metab. Reports.*, **3**, 1–4.
36. Khalighi, K., Cheng, G., Mirabbasi, S., Khalighi, B., Wu, Y. and Fan, W. (2018) Opposite impact of methylene tetrahydrofolate reductase C677T and methylene tetrahydrofolate reductase A1298C gene polymorphisms on systemic inflammation. *J. Clin. Lab. Anal.*, **32**, 2–7.
37. Le Guyader, D., Redd, M.J., Colucci-Guyon, E., Murayama, E., Kissa, K., Briolat, V., Mordeleet, E., Zapata, A., Shinomiya, H. and Herbomel, P. (2008) Origins and unconventional behavior of neutrophils in developing zebrafish. *Blood*, **111**, 132–141.
38. Massadeh, S., Umair, M., Alaamery, M. and Alfadhel, M. (2019) A novel homozygous non-sense mutation in the catalytic domain of MTHFR causes severe 5,10-methylenetetrahydrofolate reductase deficiency. *Front. Neurol.*, **10**, 1–8.
39. Chen, Z., Karaplis, A.C., Ackerman, S.L., Pogribny, I.P., Melnyk, S., Lussier-Cacan, S., Chen, M.F., Pai, A., John, S.W., Smith, R.S. *et al.* (2001) Mice deficient in methylenetetrahydrofolate reductase exhibit hyperhomocysteinemia and decreased methylation capacity, with neuropathology and aortic lipid deposition. *Hum. Mol. Genet.*, **10**, 433–443.
40. Leclerc, D., Christensen, K.E., Cauvi, O., Yang, E., Fournelle, F., Bahous, R.H., Malysheva, O.V., Deng, L., Wu, Q., Shou, Z. *et al.* (2019) Mild methylenetetrahydrofolate reductase deficiency alters inflammatory and lipid pathways in liver. *Mol. Nutr. Food Res.*, **63**, 1–12.
41. Mikael, L.G., Wang, X.L., Wu, Q., Jiang, H., Maclean, K.N. and Rozen, R. (2009) Hyperhomocysteinemia is associated with hypertriglyceridemia in mice with methylenetetrahydrofolate reductase deficiency. *Mol. Genet. Metab.*, **98**, 187–194.
42. Anderson, J., Carten, J.D. and Farber, S.A. (2016) Using fluorescent lipids in live zebrafish larvae: from imaging whole animal physiology to subcellular lipid trafficking. *Methods Cell Biol.*, **133**, 165–178.
43. Roffman, J.L., Gollu, R.L., Calhoun, V.D., Wassink, T.H., Weiss, A.P., Ho, B.C., White, T., Clark, V.P., Fries, J., Andreasen, N.C. *et al.* (2008) MTHFR 677C → T genotype disrupts prefrontal function in schizophrenia through an interaction with COMT 158Val → Met. *Proc. Natl. Acad. Sci. U. S. A.*, **105**, 17573–17578.
44. Delgado, T.C. (2013) Glutamate and GABA in appetite regulation. *Front. Endocrinol.*, **4**, 1–8.
45. Zhang, X. and van den Pol, A.N. (2016) Hypothalamic arcuate nucleus tyrosine hydroxylase neurons play orexigenic role in energy homeostasis. *Physiol. Behav.*, **19**, 1341–1347.
46. Demy, D.L., Carrere, M., Noche, R., Tauzin, M., Le Bris, M., Baek, C., Leshchiner, I., Goessling, W. and Herbomel, P. (2021) The cationic amino acid exporter Slc7a7 is induced and vital in zebrafish tissue macrophages with sustained efferocytic activity. *J. Cell Sci.*, **133**, 1–11.
47. Xu, J., Wang, T., Wu, Y., Jin, W. and Wen, Z. (2016) Microglia colonization of developing zebrafish midbrain is promoted by apoptotic neuron and lysophosphatidylcholine. *Dev. Cell*, **38**, 214–222.
48. Samaniego, R., Palacios, B.S., Domiguez-Soto, Á., Vidal, C., Salas, A., Matsuyama, T., Sánchez-Torres, C., de la Torre, I., Miranda-Carús, M.E., Sánchez-Mateos, P. and Puig-Kröger, A. (2014) Macrophage uptake and accumulation of folates are polarization-dependent in vitro and in vivo and are regulated by activin A. *J. Leukoc. Biol.*, **95**, 797–808.
49. Liu, C.C., Ho, W.Y., Leu, K.L., Tsai, H.M. and Yang, T.H. (2009) Effects of S-adenosylhomocysteine and homocysteine on DNA damage and cell cytotoxicity in murine hepatic and microglia cell lines. *J. Biochem. Mol. Toxicol.*, **23**, 349–356.
50. Rosin, J.M., Vora, S.R. and Kurrasch, D.M. (2018) Depletion of embryonic microglia using the CSF1R inhibitor PLX5622 has adverse sex-specific effects on mice, including accelerated weight gain, hyperactivity and anxiolytic-like behaviour. *Brain Behav. Immun.*, **73**, 682–697.
51. Christensen, K.E., Mikael, L.G., Leung, K.Y., Lévesque, N., Deng, L., Wu, Q., Malysheva, Q.V., Best, A., Caudill, M.A., Greene, N.D.E. and Rozen, R. (2015) High folic acid consumption leads to pseudo-MTHFR deficiency, altered lipid metabolism, and liver injury in mice. *Am. J. Clin. Nutr.*, **101**, 646–658.
52. Jiang, S., Zhao, R., Pan, M., Venners, S.A., Zhong, G. and Hsu, Y.H. (2014) Associations of MTHFR and MTRR polymorphisms with serum lipid levels in Chinese hypertensive patients. *Clin. Appl. Thromb.*, **20**, 400–410.

53. Li, W.X., Lv, W.W., Dai, S.X., Pan, M.L. and Huang, J.F. (2015) Joint associations of folate, homocysteine and MTHFR, MTR and MTRR gene polymorphisms with dyslipidemia in a Chinese hypertensive population: a cross-sectional study. *Lipids Health Dis.*, **14**, 101.
54. Quinlivan, V.H. and Farber, S.A. (2017) Lipid uptake, metabolism, and transport in the larval zebrafish. *Front. Endocrinol.*, **8**, 319.
55. Fang, L., Liu, C. and Miller, Y.I. (2014) Zebrafish models of dyslipidemia: relevance to atherosclerosis and angiogenesis. *Transl. Res.*, **163**, 99–108.
56. Chen, K., Wang, C.Q., Fan, Y.Q., Xie, Y.S., Yin, Z.F., Xu, Z.J., Zhang, H.L., Cao, J.T., Han, Z.H., Want, Y. *et al.* (2015) Optimizing methods for the study of intravascular lipid metabolism in zebrafish. *Mol. Med. Rep.*, **11**, 1871–1876.
57. Luo, Z., Lu, Z., Muhammad, I., Chen, Y., Chen, Q., Zhang, J. and Song, Y. (2018) Associations of the MTHFR rs1801133 polymorphism with coronary artery disease and lipid levels: a systematic review and updated meta-analysis. *Lipids Health Dis.*, **17**, 191.
58. Friso, S., Choi, S.W., Girelli, D., Mason, J.B., Dolnikowski, G.G., Bagley, P.J., Olivieri, O., Jacques, P.F., Rosenberg, I.H., Corrocher, R. and Selhub, J. (2002) A common mutation in the 5,10-methylenetetrahydrofolate reductase gene affects genomic DNA methylation through an interaction with folate status. *Proc. Natl. Acad. Sci. U. S. A.*, **99**, 5606–5611.
59. Pauwels, S., Ghosh, M., Duca, R.C., Bekaert, B., Freson, K., Huybrechts, I., Langie, S.A.S., Koppen, G., Devlieger, R. and Godderis, L. (2017) Maternal intake of methyl-group donors affects DNA methylation of metabolic genes in infants. *Clin. Epigenetics*, **9**, 16.
60. Cho, C.E., Pannia, E., Huot, P.S.P., Sánchez-Hernández, D., Kubant, R., Dodington, D.W., Ward, W.E., Bazinet, R.P. and Anderson, G.H. (2015) Methyl vitamins contribute to obesogenic effects of a high multivitamin gestational diet and epigenetic alterations in hypothalamic feeding pathways in Wistar rat offspring. *Mol. Nutr. Food Res.*, **59**, 476–489.
61. Han, X., Wang, B., Jin, D., Liu, K., Wang, H., Chen, L. and Zu, Y. (2021) Precise dose of folic acid supplementation is essential for embryonic heart development in zebrafish. *Biology*, **11**, 28.
62. Ma, Z., Zhu, P., Shi, H., Guo, L., Zhang, Q., Chen, Y., Chen, S., Zhang, Z., Peng, J. and Chen, J. (2019) PTC-bearing mRNA elicits a genetic compensation response via Upf3a and COMPASS components. *Nature*, **568**, 259–263.
63. Vidmar Golja, M., Šmid, A., Karas Kuželički, N., Trontelj, J., Geršak, K. and Mlinarič-Raščan, I. (2020) Folate insufficiency due to MTHFR deficiency is bypassed by 5-methyltetrahydrofolate. *J. Clin. Med.*, **9**, 2836.
64. Kao, T.T., Wang, K.C., Chang, W.N., Lin, C.Y., Chen, B.H., Wu, H.L., Shi, G.Y., Tsai, J.N. and Fu, T.F. (2008) Characterization and comparative studies of zebrafish and human recombinant dihydrofolate reductases - inhibition by folic acid and polyphenols. *Drug Metab. Dispos.*, **36**, 508–516.
65. Ma, Y., Zhang, C., Gao, X.B., Luo, H.Y., Chen, Y., Li, H.H., Ma, X. and Lu, C.L. (2015) Folic acid protects against arsenic-mediated embryo toxicity by up-regulating the expression of Dvr1. *Sci. Rep.*, **5**, 16093.
66. Wu, R.S., Lam, I.I., Clay, H., Duong, D.N., Deo, R.C. and Coughlin, S.R. (2018) A rapid method for directed gene knockout for screening in G0 zebrafish. *Dev. Cell*, **46**, 112–125.e4.
67. Hwang, W.Y., Fu, Y., Reyon, D., Maeder, M.L., Tsai, S.Q., Sander, J.D., Peterson, R.T., Yeh, J.R.J. and Joung, J.K. (2013) Efficient genome editing in zebrafish using a CRISPR-Cas system. *Nat. Biotechnol.*, **31**, 227–229.
68. Dararat, W., Lomthaisong, K. and Sanoamuang, L.O. (2012) Biochemical composition of three species of fairy shrimp (Branchiopoda: Anostraca) from Thailand. *J. Crustac. Biol.*, **32**, 81–87.
69. Gallagher, M. and Brown, W.D. (1975) Composition of San Francisco Bay brine shrimp (*Artemia salina*). *J. Agric. Food Chem.*, **23**, 630–632.
70. Potok, M.E., Nix, D.A., Parnell, T.J. and Cairns, B.R. (2013) Reprogramming the maternal zebrafish genome after fertilization to match the paternal methylation pattern. *Cell*, **153**, 759–772.
71. Wee, C.L., Song, E.Y., Johnson, R.E., Ailani, D., Randlett, O., Kim, J., Nikitchenko, M., Bahl, A., Yang, C.T., Ahrens, M.B. *et al.* (2019) A bidirectional network for appetite control in larval zebrafish. *eLife*, **8**, e43775.
72. Williams, S.Y. and Renquist, B.J. (2016) High throughput *Danio rerio* energy expenditure assay. *J. Vis. Exp.*, **107**, e53297.
73. Livak, K.J. and Schmittgen, T.D. (2001) Analysis of relative gene expression data using real-time quantitative PCR and the 2-ΔΔCT method. *Methods*, **25**, 402–408.
74. Renshaw, S.A., Loynes, C.A., Trushell, D.M.I., Elworthy, S., Ingham, P.W. and Whyte, M.K.B. (2006) Atransgenic zebrafish model of neutrophilic inflammation. *Blood*, **108**, 3976–3978.
75. Ellett, F., Pase, L., Hayman, J.W., Andrianopoulos, A. and Lieschke, G.J. (2011) Mpeg1 promoter transgenes direct macrophage-lineage expression in zebrafish. *Blood*, **117**, e49–e56.
76. de Oliveira, S., Reyes-Aldasoro, C.C., Candel, S., Renshaw, S.A., Mulero, V. and Calado, Â. (2013) Cxcl8 (IL-8) mediates neutrophil recruitment and behavior in the zebrafish inflammatory response. *J. Immunol.*, **190**, 4349–4359.
77. Tucker, B. and Lardelli, M. (2007) A rapid apoptosis assay measuring relative acridine orange fluorescence in zebrafish embryos. *Zebrafish*, **4**, 113–116.
78. Chen, B., Zheng, Y.M. and Zhang, J.P. (2018) Comparative study of different diets-induced NAFLD models of zebrafish. *Front. Endocrinol.*, **9**, 366.
79. Dai, W., Wang, K., Zheng, X., Chen, X., Zhang, W., Zhang, Y., Hou, J. and Liu, L. (2015) High fat plus high cholesterol diet lead to hepatic steatosis in zebrafish larvae: a novel model for screening anti-hepatic steatosis drugs. *Nutr. Metab.*, **12**, 42.
80. Ma, J., Yin, H., Li, M., Deng, Y., Ahmad, O., Qin, G., He, Q., Li, J., Gao, K., Zhu, J. *et al.* (2019) A comprehensive study of high cholesterol diet-induced larval zebrafish model: a short-time in vivo screening method for non-alcoholic fatty liver disease drugs. *Int. J. Biol. Sci.*, **15**, 973–983.
81. Hernandez, R.E., Galitan, L., Cameron, J., Goodwin, N. and Ramakrishnan, L. (2018) Delay of initial feeding of zebrafish larvae until 8 days postfertilization has no impact on survival or growth through the juvenile stage. *Zebrafish*, **15**, 515–518.
82. Nandania, J., Kokkonen, M., Euro, L. and Velagapudi, V. (2018) Simultaneous measurement of folate cycle intermediates in different biological matrices using liquid chromatography–tandem mass spectrometry. *J. Chromatogr. B Analyt. Technol. Biomed. Life Sci.*, **1092**, 168–178.